Separation and Purification Technology 315 (2023) 123718

Contents lists available at ScienceDirect

Separation and Purification Technology

journal homepage: www.elsevier.com/locate/seppur

# A flow-through strategy using supported ionic liquids for L-asparaginase purification

João C.F. Nunes [a], Mafalda R. Almeida [a], Gabriela B. de Paiva [b], Danielle B. Pedrolli [b], Valéria C. Santos-Ebinuma [b], Márcia C. Neves [a], Mara G. Freire [a], Ana P.M. Tavares [a,*]

[a] CICECO – Aveiro Institute of Materials, Department of Chemistry, University of Aveiro, 3810-193 Aveiro, Portugal
[b] School of Pharmaceutical Sciences, Department of Bioprocess Engineering and Biotechnology, São Paulo State University (UNESP), Araraquara, São Paulo 14800-903, Brazil

ARTICLE INFO

*Keywords:*
L-asparaginase
Semi-continuous purification
Silica-based supported ionic liquid-like phase materials
Flow-through downstream processing

ABSTRACT

L-asparaginase (ASNase) is an amidohydrolase enzyme widely distributed in nature, e.g., microorganisms, plants and tissues of several animals. Nevertheless, microorganisms are the preferential source of ASNase since they usually grow in simple substrates and culture conditions. However, a high level of enzyme purity is required by the pharmaceutical industry, in which the applied downstream process may account for up to 80% of the total ASNase production costs. Silica-based supported ionic liquid-like phase (SSILLP) materials are here proposed as alternative immobilization/capture or processing supports for the ASNase purification. SSILLP materials with different alkyl chain lengths at the cation source and $Cl^-$ as the counterion were investigated to purify ASNase by the flow-through like mode. Silica functionalized with dimethylbutylpropylammonium chloride ([Si][$N_{3114}$]Cl) was selected as the most promising material since it displayed the highest purification factor (1.65) and specific activity of ASNase (0.026 U $mg^{-1}$) achieved. The ASNase purification operating conditions were then optimized through Response Surface Methodology, using pH (range in which enzyme is active) and solid/liquid ratio (S/L ratio) as factors, achieving a maximum purification factor of 3.36. Semi-continuous purification of ASNase was finally performed under the optimized purification conditions (pH 3 and S/L ratio of 15), enabling a purification factor of 5.15. This corresponds to a 3.12- and a 1.53-fold increase in the purification factor obtained compared with the initial screening and batch assays under optimized purification conditions. These findings demonstrate that SSILLP materials can act as simple semi-continuous ASNase purification supports with potential in flow-through downstream processing.

*Abbreviations:* $A_A$, ASNase activity; ABS, Aqueous biphasic systems; ALL, Acute lymphoblastic leukemia; ANOVA, Analysis of variance; ASNase, L-asparaginase; ATR-FTIR, Attenuated total reflectance-Fourier-transform infrared; AU, Absorbance units; BA, Bonding amount; BET, Brunauer-Emmett-Teller; BJH, Barrett-Joyner-Halenda; BSA, Bovine serum albumin; [$C_3C_1$im]Cl, 1-methyl-3-propylimidazolium chloride; $C_{TP}$, Total protein concentration; DTT, Dithiothreitol; FDA, Food and Drug Administration; ILs, Ionic liquids; LB, Luria Bertani; log $K_{ow}$, Log of the octanol–water partition coefficient; $OD_{600\ nm}$, Optical density at 600 nm; PBS, Phosphate buffered saline; PF, Purification factor; pI, Isoelectric point; PZC, Point of zero charge; $R^2$, Regression coefficient; RSM, Response surface methodology; RT, Room temperature; $SA_A$, Specific ASNase activity; $SA_{AA}$, Specific ASNase activity after purification; $SA_{AB}$, Specific ASNase activity before purification; $S_{BET}$, Specific surface area; SEM, Scanning electron microscopy; SDS-PAGE, Sodium dodecyl sulfate–polyacrylamide gel electrophoresis; [Si][$C_3$]Cl, Silica with a chloropropyl spacer arm; SILs, Supported ionic liquids; [Si][$C_3C_1$im]Cl, Silica functionalized with 1-methyl-3-propylimidazolium chloride; [Si][$N_{3114}$]Cl, Silica functionalized with dimethylbutylpropylammonium chloride; [Si][$N_{3116}$]Cl, Silica functionalized with dimethylhexylpropylammonium chloride; [Si][$N_{3118}$]Cl, Silica functionalized with dimethyloctylpropylammonium chloride; [Si][$N_{3222}$]Cl, Silica functionalized with triethylpropylammonium chloride; [Si][$N_{3444}$]Cl, Silica functionalized with tributylpropylammonium chloride; [Si][$N_{3666}$]Cl, Silica functionalized with trihexylpropylammonium chloride; [Si][$N_{3888}$]Cl, Silica functionalized with trioctylpropylammonium chloride; S/L ratio, Solid/liquid ratio; SSILLP materials, Silica-based supported ionic liquid-like phase materials; TCA, Trichloroacetic acid; Tris, Tris(hydroxymethyl) aminomethane; U, Unit of ASNase activity.

* Corresponding author.
*E-mail address:* aptavares@ua.pt (A.P.M. Tavares).

https://doi.org/10.1016/j.seppur.2023.123718
Received 31 January 2023; Received in revised form 25 March 2023; Accepted 27 March 2023
Available online 31 March 2023

## 1. Introduction

L-asparaginase (ASNase, E.C.3.5.1.1) is an enzyme widely distributed in nature, being found in microorganisms, plants, and tissues (liver, pancreas, brain, ovary or testes, kidneys, spleen, and lungs) of several animals, like fishes, mammals and birds [1,2]. However, microorganisms such as bacteria, filamentous fungi, yeast, actinomycetes, and microalgae are a better source than animals or plants, due to their ability to easily grow on rather simple or inexpensive substrates [1,3]. Furthermore, they offer an easy optimization of culture conditions for enzyme bulk production, easy genetic modification to increase the yield, economically viable extraction and purification, and good stability coupled with the *ex-situ* preservation [1].

ASNase catalyzes the hydrolysis of L-asparagine into L-aspartic acid and ammonia [4,5], but can also catalyze the hydrolysis of L-glutamine into L-glutamic acid and ammonia, and β-aspartyl peptide amide into L-aspartic acid and amino acids or peptides, with lower reaction yields [6–8]. Based on the ASNase ability to catalyze L-asparagine, bacterial ASNase type II is known as a potential drug for the treatment of several diseases, namely acute lymphoblastic leukemia (ALL), autoimmune diseases related to T-cell mediated abnormal responses [9,10], and some cancers (ovarian cancer [11], breast cancer [12] and lung cancer [13]) due to its antitumor properties. Specifically, the treatment of ALL including ASNase type II (mainly in children) has drastically increased the survival rate of ALL patients, from 54% to 90% [14]. ASNase type II inhibits the growth of cancerous cells by depleting L-asparagine from the bloodstream, which is a vital nutrient for malignant or cancerous cells [15].

ASNase commercially available has been industrially produced from *Escherichia coli*, namely Elspar (the first ASNase to be commercially available and to be approved by the U.S. Food and Drug Administration (FDA) in 1978), Leukanase, Kidrolase and Oncaspar (Pegylated *E. coli* ASNase), only for patients with hypersensitivity to native Elspar [2]. However, *E. coli* ASNase type II also has glutaminase activity causing secondary adverse effects in patients, such as leucopenia, immunosuppression, acute pancreatitis, thrombolysis, hyperglycemia, and neurological seizures [9,15,16]. Moreover, the administration of *E. coli* ASNase can cause hypersensitivity reactions in 60% of the patients, resulting in mild to severe local reactions, like urticaria, bronchospasm, serum sickness, hypotension, anaphylaxis and immunosuppression [1,4,8,9].

Besides the secondary effects of *E. coli* ASNase type II, a high level of ASNase purity is required by the pharmaceutical industry, in which downstream processing may contribute from 50 to 80% of the total ASNase production costs [1]. ASNase downstream processes include enzyme extraction and purification by non-chromatographic processes (centrifugation or fractional precipitation [4]) and chromatographic processes (ion-exchange, gel filtration, and affinity chromatography [17,18]). Centrifugation is regularly applied to remove insoluble residues after ASNase production [18]. However, fermented broths where ASNase is found, contain many other proteins with similar or higher molecular weights, leading to a poor resolution [18]. To increase ASNase purity, fractional precipitation or chromatographic techniques have been applied. In the first purification strategy, the most used precipitation agent is ammonium sulfate [4]. For instance, Abd El Baky and El Baroty [19] purified ASNase from *Spirulina maxima* using 80% ammonium sulfate. In this study, a purification fold of 5.28 times higher than the crude enzyme and an enzyme yield of 91.26% were obtained. Similarly, El-Naggar et al. [17] purified ASNase from *Streptomyces fradiae* using ammonium sulphate and obtained a purification fold of 1.417 and an enzyme recovery of 8.667%. Regarding the chromatographic processes, ion exchange, affinity, and gel filtration chromatography are usually applied and used to achieve maximum purification of the enzyme [18]. Depending on the source of ASNase and the molecular weight of the enzyme, different types of chromatography columns can be selected [7]. Abd El Baky and El Baroty [19] enhanced the purification factor to 10.91 using CM-Sephadex C-200 gel filtration chromatography, while El-Naggar et al. [17] increased the purification factor to 3.338 with ion exchange chromatography through DEAE Sepharose CL-6B column. Moreover, Hassan et al. [20] purified ASNase produced by marine *Aspergillus terreus* using 65% ammonium sulphate precipitation, followed by gel filtration on Sephadex G-100 and DEAE-cellulose ion exchange chromatography. An increase in the purification by 2.75-, 5.47-, and 11.96-fold and 37.35%, 14.38%, and 14.22% of yield were, respectively, obtained. Moharib [21] also used gel filtration chromatography through Sephacryl S-200 to purify ASNase produced by *Vigna unguiculata* seed after a first step of purification by precipitation with ammonium sulphate, followed by ion-exchange chromatography through DEAE-Sepharose column. The results showed a purification fold increase from 2 to 31 with a yield reduction from 61% to 28.24%. Nickel-affinity chromatography was also applied for ASNase purification from *Bacillus amyloliquefaciens,* resulting in an enzyme purification fold of 8.26 and a yield of 30.80% [22]. The literature results on ASNase downstream processing are summarized in Table 1.

Beyond conventional methods, alternative processes for ASNase purification are being studied by the science community, such as aqueous biphasic systems (ABS) [23]. Using a polymer-salt-based ABS to purify *E. coli* ASNase, Santos et al. [23] achieved a high enzyme recovery (87.94%) and a purification factor of 20.09. Nevertheless, the development of simpler and cost-efficient techniques capable to separate, extract and purify ASNase is still an open field.

Supported ionic liquids (SILs) have been successfully employed in the immobilization/capture or purification of several biomolecules [24–29], including proteins [24,25,27] and ASNase as previously reported by our research group [26]. Ionic liquids (ILs) have been widely applied in the separation field due to their designer capacity, namely the cation and anion structures manipulation according to the desired properties and thus improving separation performance and selectivity towards a target compound [25]. This important property is also shown in silica-based supported ionic liquid-like phase (SSILLP) materials, since ILs are the functional groups of silica (the support to which they are covalently bound), allowing different interactions to be established between the target compounds and the matrix. Despite the success of SSILLP materials in the processing of biomolecules, namely in the capture of bacterial RNA [28] or purification of antibodies [25], to the best of our knowledge, they were not previously applied for the purification of enzymes.

Based on the drawbacks related to *E. coli* ASNase type II, such as the total costs of the downstream process of ASNase, its relevant application, and promising results of SSILLP materials in biomolecules processing, in this work, SSILLP materials with different alkyl chain lengths at the cation source and $Cl^-$ as the anion source were used as simple alternative supports for the semi-continuous ASNase purification.

## 2. Materials and methods

The reagents used in the synthesis of SSILLP materials were 3-chloropropyltrimethoxysilane (≥98% pure) and tributylamine (99% pure) acquired from Acros Organics-Thermo Fisher Scientific (Bridgewater, NJ, USA); ethanol (≥99.8% pure) and trioctylamine (≥98% pure) provided by Honeywell Research Chemicals-Inc. Fluka (Charlotte, NC, USA); hydrochloric acid (HCl, 37% w/w), N,N-dimethylbutylamine (≥98.5% pure), N,N-dimethylhexylamine (≥97.5% pure), N,N-dimethyloctylamine (≥94% pure), and trihexylamine (≥95.5% pure) purchased from Sigma-Aldrich-Merck KgaA (St. Louis, MI, USA); and methanol (≥99.9% pure), toluene (≥99.8% pure), and triethylamine (≥99% pure) obtained from Thermo Fisher Scientific (Waltham, MA, USA).

For the production of ASNase, the following reagents were used: glycerol (analytical reagent) acquired from Biochem Chemopharma (Cosne-Cours-sur-Loire, France); and Luria Bertani (LB) broth (Lennox) (for molecular biology), erythromycin (for cell culture), D-(+)-Xylose

**Table 1**
ASNase downstream processes: non-chromatographic and chromatographic processes, ASNase source, and purification factor.

| ASNase downstream process | | ASNase source | Purification factor | Ref. |
|---|---|---|---|---|
| Non-chromatographic process | Chromatographic process | | | |
| Ammonium sulfate precipitation | – | *S. maxima* | 5.28 | [19] |
| | CM-Sephadex C-200 gel filtration | | 10.91 | |
| Ammonium sulfate precipitation | – | *S. fradiae* | 1.417 | [17] |
| | DEAE Sepharose CL-6B ion exchange chromatography | | 3.338 | |
| Ammonium sulphate precipitation | – | *A. terreus* | 2.75 | [20] |
| | Sephadex G-100 gel filtration – | | 5.47 | |
| | DEAE-cellulose ion exchange chromatography | | 11.96 | |
| Ammonium sulphate precipitation | – | *V. unguiculata* | 2 | [21] |
| | DEAE-Sepharose column ion exchange chromatography Sephacryl S-200 column gel filtration | | 31 | |
| – | Ni-sepharose 6 FF affinity chromatography | *B. amyloliquefaciens* | 8.26 | [22] |

(≥99% pure), and phosphate-buffered saline (PBS) tablets provided by Sigma-Aldrich-Merck KGaA (St Louis, MO, USA).

To determine ASNase activity, the following reagents were applied: L-asparagine (99% pure) purchased from Acros Organics-Thermo Fisher Scientific (Bridgewater, NJ, USA); Tris(hydroxymethyl) aminomethane (Tris, 99% pure) obtained from Alfa Aesar-Thermo Fisher Scientific (Kandel, Germany); Trichloroacetic acid (TCA, 99.5% pure) acquired from Sigma-Aldrich-Merck KGaA (St Louis, MO, USA); and Nessler's reagent (pure) provided by PanReac AppliChem ITW Reagents (Darmstadt, Germany).

### 2.1. SSILLP materials synthesis

Seven SSILLP materials with quaternary ammonium cations with different alkyl chain lengths and chloride as the counterion were synthesized using an adaptation of the protocol detailed by Qiu et al. [30], corresponding to dimethylbutylpropylammonium chloride ([Si][$N_{3114}$]Cl), dimethylhexylpropylammonium chloride ([Si][$N_{3116}$]Cl), dimethyloctylpropylammonium chloride ([Si][$N_{3118}$]Cl), triethylpropylammonium chloride ([Si][$N_{3222}$]Cl), tributylpropylammonium chloride ([Si][$N_{3444}$]Cl), trihexylpropylammonium chloride ([Si][$N_{3666}$]Cl), and trioctylpropylammonium chloride ([Si][$N_{3888}$]Cl). The synthesis of the SSILLP materials was carried out through two main steps: (i) commercial silica gel 60 (0.2–0.5 mm) activation with a hydrochloric acid (37%w/w) treatment for 24 h to enhance the silanol groups content on the silica surface and (ii) silica functionalization, comprising two reactions: the first reaction with a silane-coupling agent that also provides the anion (3-chloropropyltrimethoxysilane, $C_6H_{15}ClO_3Si$), followed by a second reaction with the cation source. To this end, 5 g of the activated silica was suspended in 60 mL of toluene and 5 mL of $C_6H_{15}ClO_3Si$ was added. This suspension was kept under reflux and magnetic stirring for 24 h. Then, the resulting solid was filtrated and washed by the following order: 100 mL of toluene, 200 mL of ethanol:water 1:1 (v/v), 500 mL of distilled water, and 100 mL of methanol, and dried for 24 h at 60 °C, resulting in silica with a chloropropyl spacer arm ([Si][$C_3$]Cl). For the second reaction of the silica functionalization, 5 g of [Si][$C_3$]Cl were mixed with 60 mL of toluene, and 5 mL of the cation source, e.g., N,N-dimethylbutylamine, and kept under reflux and magnetic stirring for 24 h. Afterwards, the material was filtrated and washed using the following sequence: 100 mL of toluene, 350 mL of methanol, 300 mL of distilled water, and 150 mL of methanol, and dried for 24 h at 60 °C.

### 2.2. Characterization of SSILLP materials

All synthesized SSILLP materials ([Si][$N_{3114}$]Cl, [Si][$N_{3116}$]Cl, [Si][$N_{3118}$]Cl, [Si][$N_{3222}$]Cl, [Si][$N_{3444}$]Cl, [Si][$N_{3666}$]Cl, and [Si][$N_{3888}$]Cl) were characterized through elemental analysis and zeta potential analysis to determine the point of zero charge (PZC). All SSILLP materials were also characterized before contact with the enzymatic extract (except for [Si][$N_{3114}$]Cl which was characterized before and after contact with the enzymatic extract), through Attenuated total reflectance-Fourier-transform infrared (ATR-FTIR) spectroscopy, Brunauer-Emmett-Teller (BET) and Barrett-Joyner-Halenda (BJH) analysis. The SSILLP material selected as the best to be further applied in the optimization of ASNase purification, i.e., [Si][$N_{3114}$]Cl was also characterized through scanning electron microscopy (SEM).

#### 2.2.1. Elemental analysis

The weight percentages (%w/w) of carbon (%C), hydrogen (%H), and nitrogen (%N) of all SSILLP materials were determined through elemental analysis using 2 mg of each sample, the equipment TruSpec 630–200-200, and 1075 °C and 850 °C as the respective combustion furnace and subsequent burner temperature. Infrared absorption was the detection method for carbon and hydrogen, while thermal conductivity was the detection method for nitrogen.

The bonding amount (BA) (μmol $m^{-2}$) of ILs onto all SSILLP materials was calculated considering the amount of nitrogen present, according to Eq. (1).

$$BA = \frac{\frac{\%N}{M(N)\times 100}}{S_{BET}} \quad (1)$$

where %N is the weight percentage of nitrogen, M(N) is the molar mass of nitrogen (g $\mu mol^{-1}$), and $S_{BET}$ is the specific surface area of the activated silica (494.2 $m^2$ $g^{-1}$).

The mass of IL per mass of material (mg $g^{-1}$) of all SSILLP materials was calculated considering the amount of nitrogen present, according to Eq. (2).

$$\text{IL mass per material mass} = \frac{\frac{\%N\times M_{IL}}{N_{IL}}}{100}\times 1000 \quad (2)$$

where %N is the weight percentage of nitrogen, $M_{IL}$ is the IL molar mass (g $mol^{-1}$), and $N_{IL}$ is the nitrogen mass per IL (g).

#### 2.2.2. Point of zero charge (PZC)

The PZC of activated silica and all SSILLP materials were obtained using zeta potential measurements (Malvern Zetasizer Nano ZS (Malvern Instruments Ltd., Malvern, UK)) of aqueous suspensions of each material in a wide range of pH values. Aqueous solutions of NaOH and HCl at 0.1 M and 0.01 M were used to adjust the pH of the materials' suspensions.

#### 2.2.3. Attenuated total reflectance-Fourier-transform infrared (ATR-FTIR) spectroscopy

ATR-FTIR was performed using a solid sample of activated silica and each synthesized SSILLP material, and for [Si][$N_{3114}$]Cl before and after contact with enzymatic extract, using a Perkin Elmer FT-IR System Spectrum BX (Waltham, MA, USA) equipment at 25 °C and in a range

between 4000 and 500 $cm^{-1}$. The samples were scanned 256 times with a resolution of 8.0 $cm^{-1}$.

#### 2.2.4. Brunauer-Emmett-Teller (BET) and Barrett-Joyner-Halenda (BJH) analysis

The specific surface area ($S_{BET}$) of activated silica and all SSILLP materials, including [Si][$N_{3114}$]Cl before and after contact with enzymatic extract, were assessed by gas adsorption using a Gemini V-2380 surface area analyzer (Micromeritics, Norcross, GA, USA) and determined through the BET equation with multipoint adsorption isotherms of $N_2$ at −196 °C. The pore structure characterization, i.e., pore surface area, pore volume and average pore size were estimated by the BJH model [31]. The samples were degassed overnight at room temperature before the measurements.

#### 2.2.5. Scanning electron microscopy (SEM)

SEM of activated silica and [Si][$N_{3114}$]Cl was carried out using a Hitachi S4100 microscope (Hitachi, Tokyo, Japan); a carbon thin film deposition was used to enhance the samples' conductivity.

### 2.3. ASNase production

ASNase production was performed according to the protocol previously reported by Bento et al. [32]. Briefly, the inoculum was prepared by the activation of a stock culture of *B. subtilis* (20% v/v in glycerol aqueous solution maintained at −80 °C) in 15 mL of LB medium supplemented with erythromycin 1 μg $mL^{-1}$ in 50 mL falcon tubes. Cells were grown at 37 °C, overnight (14–16 h) in an orbital shaker (Excella E24, New Brunswick Scientific, USA). The process of ASNase production was initiated by transferring the inoculum culture of *B. subtilis* to 1 L Erlenmeyer flasks containing 250 mL of LB medium and adjusting the initial optical density at 600 nm ($OD_{600\ nm}$) to 0.1 absorbance units (AU). This culture was grown at 37 °C and 220 rpm. The optical density was measured in a spectrophotometer equipment (Shimadzu UV-1800, Shimadzu Corp., Japan). When cultures reached $OD_{600\ nm}$ between 0.7 and 1 AU, 0.5% w/v of an aqueous xylose solution (50% w/v, inducing agent) was added to induce ASNase production. The bioprocess was performed at 30 °C and 220 rpm for 24 h. After cultivation, cells were harvested by centrifugation at 5000 rpm for 20 min at 25 °C. The resulting pellets were resuspended in 10 mL PBS buffer and submitted to ultrasound sonication (Branson 450 Digital Sonifier, Branson Ultrasonics Corporation, USA) with 60% power in 40 sets of 5 s pulse and 10 s intervals between them in ice bath. The enzymatic extract was recovered by centrifugation at 5000 rpm for 10 min at 25 °C.

### 2.4. Screening of SSILLP materials with different alkyl chain lengths for ASNase purification

The ASNase purification was performed through the addition of 1 mL of enzymatic extract (containing ASNase and other proteins (impurities), total protein concentration of 15 mg $mL^{-1}$) to 10 mg of the SSILLP materials with different alkyl chain lengths ([Si][$N_{3114}$]Cl, [Si][$N_{3116}$]Cl, [Si][$N_{3118}$]Cl, [Si][$N_{3222}$]Cl, [Si][$N_{3444}$]Cl, [Si][$N_{3666}$]Cl, and [Si][$N_{3888}$]Cl). The enzymatic extracts were further stirred using a programmable rotator Multi Bio RS-24 with PRS-26 platform (BioSan SIA, Riga, Latvia) for 60 min at 25 °C, and, afterwards, centrifuged (Micro Star 17, VWR, part of Avantor, Radnor, PA, USA) for 10 min at 12000 rpm aiming to separate the material from the supernatant. All purification tests were performed in duplicate.

### 2.5. Determination of ASNase activity

The ASNase activity in the supernatants was measured according to the method described by Magri et al. [33]. To determine ASNase activity, 500 μL of the enzymatic extract or supernatants (after contact with [Si][$N_{3114}$]Cl), 500 μL of 50 mM Tris-HCl pH 8.6, and 50 μL of 189 mM L-asparagine were mixed and incubated for 30 min at 37 °C. The enzymatic reaction was stopped by the addition of 250 μL of 1.5 M TCA. After centrifugation at 12,000 rpm for 10 min, samples were analyzed by the Nessler method regarding the ammonium released in the hydrolysis of L-asparagine by ASNase, directly proportional to the ASNase activity. For this, 500 μL of the stopped reaction sample, 500 μL of distilled water, and 250 μL of Nessler's reagent were mixed and incubated for 30 min at room temperature (RT). The absorbance of the sample was determined at 436 nm using a multimode microplate reader (Synergy HT, BioTek, USA). A calibration curve was previously established using ammonium sulfate. ASNase activity ($A_A$) was calculated according to Eq. (3).

$$A_A = \frac{NH_4^+ \times V_R \times V_N}{V_S \times R_T \times V_E} \quad (3)$$

where $NH_4^+$ is the ammonium concentration produced in the enzymatic reaction (μmol $mL^{-1}$), $V_R$ is the enzymatic reaction volume (1.05 mL), $V_N$ is the Nessler reaction volume (1.25 mL), $V_S$ is the stopped reaction sample volume (0.5 mL), $R_T$ is the reaction time (30 min), and $V_E$ is the enzymatic extract volume (0.5 mL). One unit of ASNase activity (U) corresponds to 1 μmol of ammonium produced per min at pH 8.6 and 37 °C.

### 2.6. Determination of total protein concentration

The protein content in the enzymatic extract was determined by spectroscopy at 280 nm using a multimode microplate reader (Synergy HT, BioTek, USA), and the total protein concentration was calculated based on a calibration curve previously established using bovine serum albumin (BSA).

### 2.7. Determination of the specific ASNase activity and purification factor

The specific ASNase activity ($SA_A$) was calculated according to Eq. (4), and it is expressed in U $mg^{-1}$.

$$SA_A = \frac{A_A}{C_{TP}} \quad (4)$$

where $A_A$ is the ASNase activity (U $mL^{-1}$), and $C_{TP}$ is the total protein concentration (mg $mL^{-1}$).

The purification factor ($P_F$) was calculated according to Eq. (5),

$$P_F = \frac{SA_{AA}}{SA_{AB}} \quad (5)$$

where $SA_{AA}$ is the specific ASNase activity after purification (U $mg^{-1}$), and $SA_{AB}$ is the specific ASNase activity before purification (U $mg^{-1}$).

### 2.8. Response surface methodology (RSM)

Following the initial screening using SSILLP materials with different alkyl chain lengths, [Si][$N_{3114}$]Cl was selected as the best SSILLP material to be further applied in the optimization of ASNase purification from the enzymatic extract. The pH and solid–liquid ratio (S/L ratio) were the factors chosen to be applied in a $2^2$ factorial planning. To adjust the pH of the enzymatic extract, aqueous solutions of HCl at 0.1 M and 1 M were used. The $2^2$ factorial planning has been defined by a central point (level zero), the factorial points (1 and −1, level one) and the axial points (level α) (Table S1 in the Supplementary Material). The equations and independent variables coded levels used in the factorial planning are given in the Supplementary Material (Table S2, Eqs. (S1-S2)). The analysis of the Response surface methodology (RSM) curves leads to the determination of the optimal conditions for ASNase purification. This planning enables the analysis of distinct operating conditions simultaneously and the identification of the most significant parameter to enhance the purification factor. The pH values of 3 and 7 represent pH 2.9 and pH 7.1 throughout the manuscript.

The enzymatic extracts were mixed using a programmable rotator Multi Bio RS-24 with PRS-26 platform (BioSan SIA, Riga, Latvia) for 60 min at 25 °C. The statistical analysis and representing response surfaces of the obtained data were performed using the Statsoft Statistica 10.0 software. The obtained results were statistically analyzed with a confidence level of 95%, and a student *t*-test was used to verify the statistical significance of the adjusted data (Table S4 in the Supplementary Material). The lack of fit, the regression coefficient ($R^2$) and the F-value obtained from the analysis of variance (ANOVA) were evaluated to determine the adequacy of the model.

### 2.9. Semi-continuous purification of ASNase

Semi-continuous purification of ASNase was performed using disposable polypropylene columns (Bio-Rad, California, USA) packed with 225 mg of [Si][$N_{3114}$]Cl (SSILLP material that enabled the highest purification of ASNase during the batch assays) under the optimized purification conditions (pH 3 and S/L ratio of 15) throughout 15 mL of enzymatic extract. The enzymatic extract was constantly supplied through a peristaltic pump (FH100, Thermo Fisher Scientific, USA) at 4 rpm. All semi-continuous purification tests were performed in duplicate. The enzymatic extract and purified cell extract fractions (separate 1st, 2nd and 3rd 5 mL of cell extract recovered following semi-continuous purification) were analyzed by sodium dodecyl sulfate–polyacrylamide gel electrophoresis (SDS-PAGE).

### 2.10. Sodium dodecyl sulfate–polyacrylamide gel electrophoresis (SDS-PAGE)

The protein profile of the enzymatic extract and purified cell extract fractions were analyzed by SDS-PAGE. The samples were diluted 1:1 (v/v) in a sample buffer comprising 0.5 M Tris-HCl pH 6.8 1:4 (v/v), SDS 10% (w/v) 2:5 (v/v), glycerol 1:5 (v/v), bromophenol blue 1:5 (w/v) and dithiothreitol (DTT, 3.1 mg per 100 μL). Following dilution, samples were heated at 95 °C for 5 min. All samples were loaded (20 μL) on Novex™ WedgeWell™ 16%, Tris-Glycine, 1.0 mm polyacrylamide gels (Invitrogen™, Massachusetts, USA). Electrophoresis was run at 100 V for 90 min. The running buffer used was Novex™ Tris-Glycine SDS running buffer 10X (Invitrogen™, Massachusetts, USA). The gels were stained with Coomassie brilliant blue. NZYColour Protein Marker I was used as molecular weight marker and commercial ASNase (P1321) (>96.0% pure) from *E. coli* ASI.357 (BioVision Inc., Massachusetts, USA) was used as ASNase standard.

## 3. Results and discussion

### 3.1. Characterization of SSILLP materials

The elemental analysis was carried out to determine the content of carbon, hydrogen, and nitrogen of activated silica and all synthesized SSILLP materials, whose results are presented in Table 2. All SSILLP materials comprise carbon, hydrogen, and nitrogen, whose weight percentages range from 5.64 to 10.89%, from 1.38 to 3.17%, and from 0.13 to 1.06%, respectively. These results confirm the successful IL covalent binding to the silica surface, which did not contain carbon, hydrogen, and nitrogen. As previously reported by us [26], the same volume of the amines solution applied in the synthesis resulted in distinct functionalization degrees, detectable through the distinct weight percentage of nitrogen, bonding amount and IL mass per material mass. Moreover, there was no linear dependence identified between the molar amount of the cation source and the bonding amount of IL per material mass. The highest molar amounts (0.04 mol) used in the synthesis of [Si][$N_{3114}$]Cl and [Si][$N_{3222}$]Cl resulted in distinct bonding amounts, i.e., 1.53 and 0.56 μmol $m^{-2}$, and IL mass per material mass, i.e., 134.74 and 49.57 mg $g^{-1}$, likely due to stereochemical effects.

In order to determine the PZC of the materials, zeta potential value changes as a function of pH were assessed. Graphical representations are given in the Supplementary Material (Fig. S1), being the respective results summarized in Table 2. All SSILLP materials present higher PZC values, ranging from 6.5 to 10.8, than activated silica (3.0). Therefore, the SSILLP materials surface is more positively charged, which is due to the IL cation bound to the silica surface, further proving the successful SSILLP materials' functionalization. The PZC results of the materials under study are within the range of values previously reported by our research group [25,26,28,34]. However, an exception was observed for [Si][$N_{3114}$]Cl and [Si][$N_{3666}$]Cl since a slight increase of PZC values was detected, and which is due to the higher functionalization degrees and bonding amounts obtained for these materials.

The ATR-FTIR spectra of activated silica and all synthesized SSILLP materials, comprising [Si][$N_{3114}$]Cl before and after contact with enzymatic extract, are given in Fig. 1. The broad band present in the ATR-FTIR spectra of all SSILLP materials, between 1100 and 1000 $cm^{-1}$ (Fig. 1, dashed yellow line), corresponds to the siloxane groups (Si-O-Si) of silica (Fig. 1 - A I). The broad band detected in the ATR-FTIR spectrum of [Si][$N_{3114}$]Cl after contact with enzymatic extract between 1700 and 1600 $cm^{-1}$ (Fig. 1 - A III, dotted green line), in contrast with the spectrum of [Si][$N_{3114}$]Cl (Fig. 1 - A II, dotted green line), corresponds to the amide group of the polypeptide chain of protein impurities, thus supporting the adsorption of impurities onto [Si][$N_{3114}$]Cl.

The specific surface area of activated silica and all SSILLP materials were evaluated through gas adsorption and determined by the BET equation. The results are summarized in Table 3. All SSILLP materials have a lower specific surface area, ranging from 171.7 to 375.1 $m^2\ g^{-1}$, than activated silica (494.2 $m^2\ g^{-1}$). The specific surface area decreases are in accordance with the ones previously reported for [Si][$N_{3114}$]Cl, [Si][$N_{3444}$]Cl, and [Si][$N_{3888}$]Cl [34], suggesting the IL covalent bound to the silica surface and confirming the successful SSILLP materials' functionalization. The pore surface area and pore volume of all SSILLP materials estimated by the BJH model were also lower, ranging from 246.2 to 481.0 $m^2\ g^{-1}$ and from 0.33 to 0.55 $cm^3\ g^{-1}$, than obtained for activated silica (553.0 $m^2\ g^{-1}$, 0.76 $cm^3\ g^{-1}$). Both pore surface area and pore volume reductions are in accordance with the ones previously reported for imidazolium-based materials, such as silica functionalized with 1-methyl-3-propylimidazolium chloride ([Si][$C_3C_1$im]Cl) [35], suggesting the covalent bound of IL on the pore walls.

The pore surface area (292.9–304.7 $m^2\ g^{-1}$) and pore volume

**Table 2**
Weight percentages of carbon (%C), hydrogen (%H), and nitrogen (%N); molar amount (n (mol)) of each amine used for the synthesis; bonding amount (BA) (μmol $m^{-2}$); mass of ionic liquid (IL) per mass of material (i.e., silica) (mg $g^{-1}$); and point of zero charge (PZC) of activated silica and all SSILLP materials.

| Material | %C | %H | %N | n (mol) | BA (μmol $m^{-2}$) | IL mass per material mass (mg $g^{-1}$) | PZC |
|---|---|---|---|---|---|---|---|
| Silica | – | – | – | – | – | – | 3.0 |
| [Si][$N_{3114}$]Cl | 9.43 | 3.17 | 1.06 | 0.04 | 1.53 | 134.74 | 10.1 |
| [Si][$N_{3116}$]Cl | 10.49 | 2.96 | 0.95 | 0.03 | 1.37 | 139.88 | 10.8 |
| [Si][$N_{3118}$]Cl | 10.89 | 1.63 | 0.76 | 0.02 | 1.09 | 126.83 | 10.6 |
| [Si][$N_{3222}$]Cl | 6.38 | 2.34 | 0.39 | 0.04 | 0.56 | 49.57 | 9.3 |
| [Si][$N_{3444}$]Cl | 6.62 | 1.57 | 0.18 | 0.02 | 0.26 | 34.16 | 7.1 |
| [Si][$N_{3666}$]Cl | 6.12 | 1.51 | 0.14 | 0.01 | 0.20 | 34.07 | 6.8 |
| [Si][$N_{3888}$]Cl | 5.64 | 1.38 | 0.13 | 0.01 | 0.19 | 41.41 | 6.5 |

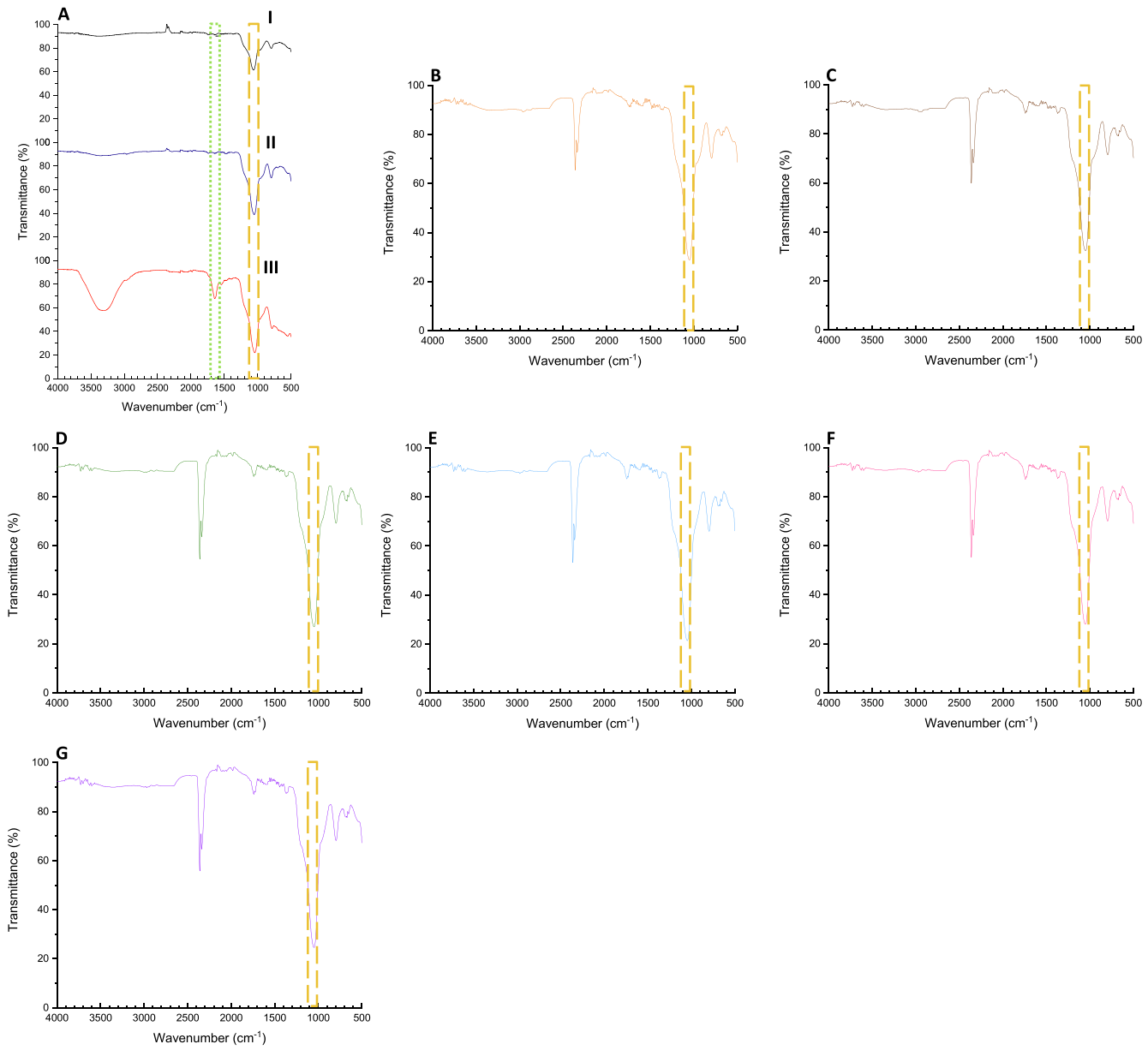


**Fig. 1.** Attenuated total reflectance-Fourier-transform infrared (ATR-FTIR) spectra of silica (A I), [Si][$N_{3114}$]Cl (A II), [Si][$N_{3114}$]Cl after contact with enzymatic extract (A III), [Si][$N_{3116}$]Cl (B), [Si][$N_{3118}$]Cl (C), [Si][$N_{3222}$]Cl (D), [Si][$N_{3444}$]Cl (E), [Si][$N_{3666}$]Cl (F), and [Si][$N_{3888}$]Cl (G). 1700–1600 $cm^{-1}$, amide group of the polypeptide chain of protein impurities (dotted green line); 1100–1000 $cm^{-1}$, siloxane groups (Si-O-Si) of silica (dashed yellow line).

**Table 3**
Specific surface area ($S_{BET}$); Barrett-Joyner-Halenda (BJH) adsorption cumulative pore surface area ($m^2\ g^{-1}$), pore volume ($cm^3\ g^{-1}$), and average pore size (Å) of activated silica and all SSILLP materials.

| Material | $S_{BET}$ ($m^2\ g^{-1}$) | Pore surface area ($m^2\ g^{-1}$) | Pore volume ($cm^3\ g^{-1}$) | Pore size (Å) |
|---|---|---|---|---|
| Silica | 494.2 | 553.0 | 0.76 | 55.0 |
| [Si][$N_{3114}$]Cl | 212.3[1] | 292.9[1] | 0.41[1] | 56.0[1] |
| | 215.9[2] | 304.7[2] | 0.42[2] | 54.8[2] |
| [Si][$N_{3116}$]Cl | 171.7 | 246.2 | 0.33 | 53.9 |
| [Si][$N_{3118}$]Cl | 181.3 | 259.4 | 0.33 | 51.6 |
| [Si][$N_{3222}$]Cl | 310.1 | 418.7 | 0.51 | 48.4 |
| [Si][$N_{3444}$]Cl | 308.2 | 410.3 | 0.47 | 46.1 |
| [Si][$N_{3666}$]Cl | 327.0 | 442.4 | 0.51 | 46.3 |
| [Si][$N_{3888}$]Cl | 375.1 | 481.0 | 0.55 | 45.9 |

*Before[1] and after[2] contact with the enzymatic extract.

(0.41–0.42 $cm^3\ g^{-1}$) of [Si][$N_{3114}$]Cl was the same before and after contact with enzymatic extract, supporting that the adsorption of impurities occurs on the surface of this material and not inside the pores. The average pore size was similar for activated silica and [Si][$N_{3114}$]Cl (54.8–56.0 Å). Moreover, there were no major differences in the average pore size of the remaining SSILLP materials, i.e., [Si][$N_{3116}$]Cl, [Si][$N_{3118}$]Cl, [Si][$N_{3222}$]Cl, [Si][$N_{3444}$]Cl, [Si][$N_{3666}$]Cl, and [Si][$N_{3888}$]Cl (45.9–53.9 Å), and activated silica (55.0 Å) (Table 3), supporting that the IL functionalization of silica does not significantly change the pore size of the materials.

SEM was carried out to assess the morphology of [Si][$N_{3114}$]Cl. SEM images of activated silica and [Si][$N_{3114}$]Cl are given in Fig. 2. SEM images of activated silica show that silica has a heterogeneous particle size and morphology. Nevertheless, SEM images of [Si][$N_{3114}$]Cl display that this material has a surface with lower roughness likely due to the existence of organic moieties at its surface, as previously reported for imidazolium-based SILs [35]. Overall, SSILLP materials'

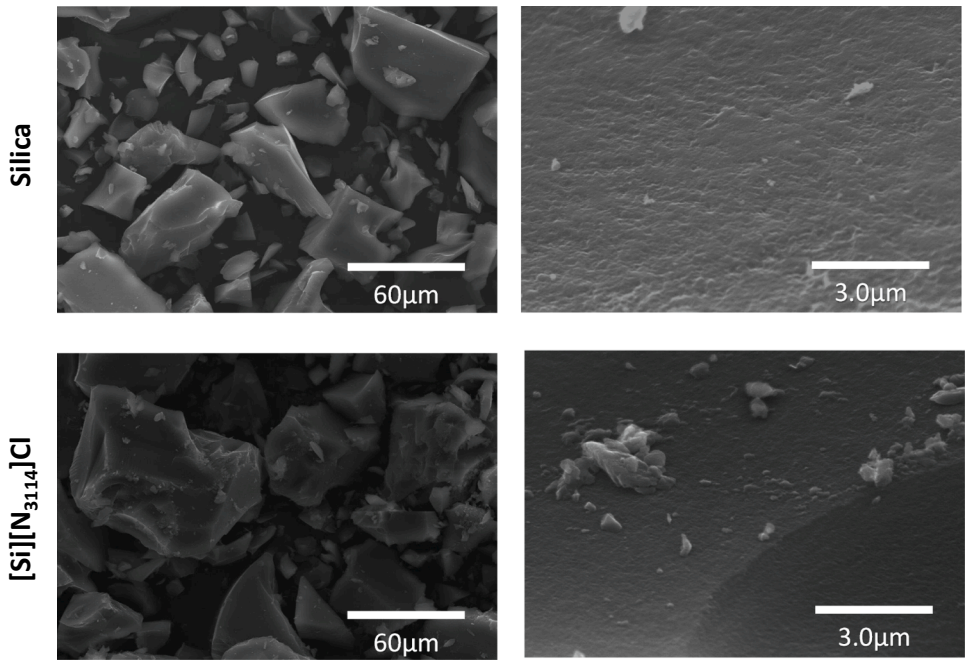


**Fig. 2.** Scanning electron microscopy (SEM) images of activated silica and [Si][$N_{3114}$]Cl.

characterization through elemental analysis, PZC, ATR-FTIR spectroscopy, BET and BJH analysis, and SEM enabled to confirm the successful materials' functionalization.

### 3.2. Screening of SSILLP materials with different alkyl chain lengths for ASNase purification

Seven different amines were assessed as cations due to the potential of ammonium-based ILs in protein immobilization/capture [25,26]. Chloride was selected as the counterion in all SSILLP materials to avoid the use of more complex anions, and to reduce the cost of the materials and their eco- and cytotoxicity [25,34]. An initial screening of the SSILLP materials with different alkyl chain lengths was carried out to assess the most promising SSILLP material for the purification of ASNase from *Aliivibrio fischeri* by the flow-through elution mode. The schematic representation of the proposed ASNase purification process mediated by

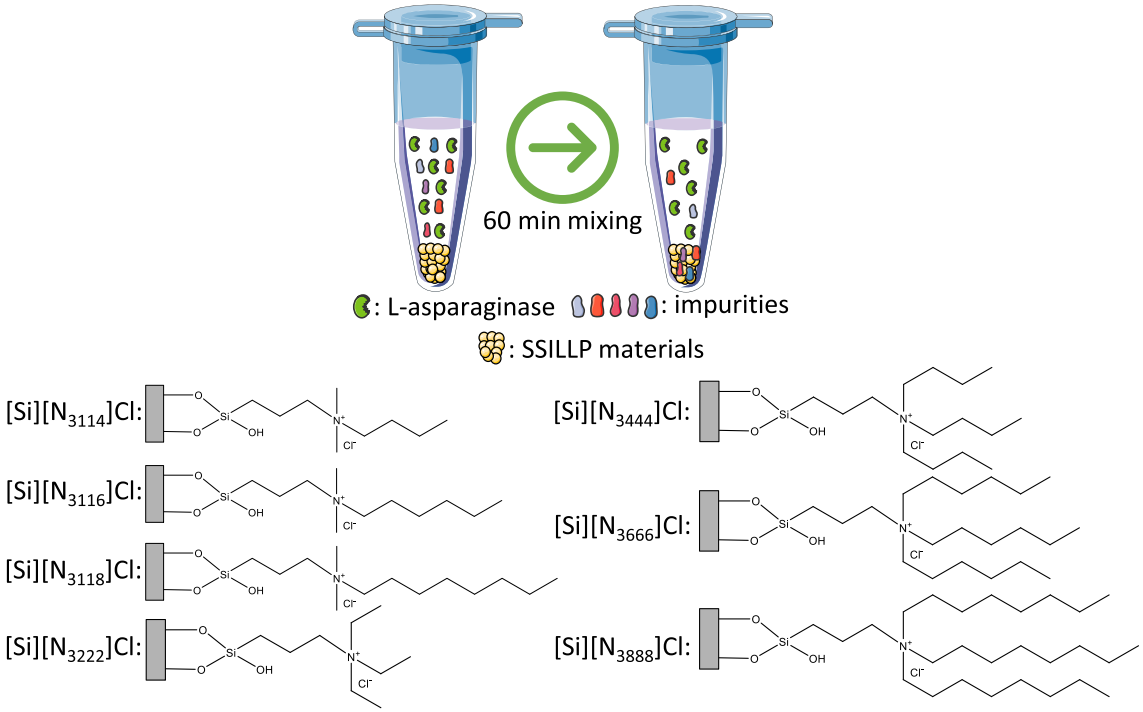


**Fig. 3.** Schematic representation of the proposed ASNase purification process mediated by SSILLP materials: protein impurities adsorbed on SSILLP materials while L-asparaginase remains in solution. Abbreviation and chemical structure of the SSILLP materials used are also provided ([Si][$N_{3114}$]Cl, [Si][$N_{3116}$]Cl, [Si][$N_{3118}$]Cl, [Si][$N_{3222}$]Cl, [Si][$N_{3444}$]Cl, [Si][$N_{3666}$]Cl and [Si][$N_{3888}$]Cl) (The Fig. 3 was partly generated using Servier Medical Art, provided by Servier, licensed under a Creative Commons Attribution 3.0 unported license).

SSILLP materials, and abbreviation and chemical structure of the SSILLP materials used are given in Fig. 3.

Operating conditions, namely pH of 7.4, S/L ratio of 10:1 (mg $mL^{-1}$), and 60 min at 25 °C, were kept constant in all experiments. The ASNase activity and total protein concentration were measured in the enzymatic extract and supernatants (after contact with the SSILLP materials). The effect of different alkyl chain lengths on the purification factor and specific activity of ASNase is given in Fig. 4. The ASNase purification factor increases from 1.26 to 1.65, with protein impurities being adsorbed on the SSILLP material and ASNase being kept in the supernatant. The specific activity of ASNase ranged from 0.013 U $mg^{-1}$ to 0.026 U $mg^{-1}$.

As previously proposed by us [26], hydrophobic interactions are the main driving forces involved in the immobilization by physical adsorption of ASNase over SSILLP materials when using a simple buffer solution containing pure commercial ASNase from *E. coli* ASI.357. When using a complex extract after cell lysis containing ASNase and other proteins (impurities), while attempting the flow-through elution mode, the lowest purification factors (1.26, 1.26, and 1.35) and specific activity of ASNase (0.013 U $mg^{-1}$, 0.013 U $mg^{-1}$, and 0.014 U $mg^{-1}$) were obtained using the most hydrophobic SSILLP materials, comprising the IL with the longest alkyl chain lengths i.e., [Si][$N_{3444}$]Cl, [Si][$N_{3666}$]Cl, and [Si][$N_{3888}$]Cl, respectively. On the other hand, the highest purification factor (1.65) and specific activity of ASNase (0.026 U $mg^{-1}$) were obtained using the least hydrophobic SSILLP material, comprising the IL with the shortest alkyl chain length, i.e., [Si][$N_{3114}$]Cl. The log of the octanol–water partition coefficient (log $K_{ow}$) of the cation N,N-dimethylbutylamine (1.60) is much lower than the log $K_{ow}$ of the cation trioctylamine (9.45), further proving [Si][$N_{3114}$]Cl as the least hydrophobic SSILLP material under study [36]. These results, together with our previous findings where the goal was to adsorb ASNase [26], support the existence of preferential hydrophobic interactions between ASNase and the SSILLP materials. Comparing the best purification factor of 1.65 with that obtained with activated silica, i.e., 1.03, an increase of 1.60-fold is achieved, supporting the importance of silica functionalization with ILs for the purification of ASNase. Based on this set of results, [Si][$N_{3114}$]Cl was chosen for the following assays since it displays a higher affinity to the impurities present in the enzymatic extract over ASNase.

### 3.3. Optimization of ASNase purification conditions through RSM

To identify the optimal ASNase purification operating conditions from the enzymatic extract, it is required to take into account the interactions between factors, namely pH and S/L ratio. The pH was selected due to the importance of possible electrostatic interactions between ASNase or other proteins and the [Si][$N_{3114}$]Cl. The reported ASNase isoelectric point (pI) is between 5.0 and 5.7 [37], and the PZC value of [Si][$N_{3114}$]Cl under study is 10.1, as given in Table 2. Therefore, a pH range between pH 3.0 and pH 7.0 comprises similar and opposite charges of the enzyme and the material since; from pH 3.0 to pH 4.9, both ASNase and [Si][$N_{3114}$]Cl are positively charged; and from pH 5.8 to pH 7.0, ASNase is negatively charged and [Si][$N_{3114}$]Cl is positively charged, as detailed in Fig. 5. It is important to highlight that the enzyme is active in this pH range (ASNase activity of enzymatic extract at pH 3 and RT: 0.082 U $mL^{-1}$) – data provided in the Supplementary Material (Fig. S5). RSM was applied using a $2^2$ factorial planning (2 factors and 2 levels). The results obtained via RSM are given in Fig. 6. ANOVA was applied in order to estimate the statistical significance of variables and the interactions among them. The experimental conditions and purification factor values experimentally obtained using [Si][$N_{3114}$]Cl and the respective calculated values, in addition to the complete statistical analysis, are given in the Supplementary Material (Tables S1–S5 and Figs. S2–S4).

The results depicted in Fig. 6 show that when using low medium pH and higher S/L ratio, higher purification factors are obtained. The pH effect is the only significant variable with a linear, negative effect regarding the ASNase purification factor, as shown in the Pareto chart given in the Supplementary Material (Fig. S2). Therefore, the predicted optimal experimental conditions to enhance the purification factor were a pH value of 3 and S/L ratio of 15 (Fig. S4 in the Supplementary Material). These predicted optimal conditions were experimentally assessed without significant differences between the predicted (purification factor of 3.69) and the experimentally obtained results (purification factor of 3.36). In fact, comparing the initial screening to batch assay under optimized purification conditions, there was a 2.03-fold increase in the ASNase purification factor attained. At pH 3.0, both ASNase and [Si][$N_{3114}$]Cl are positively charged, suggesting that electrostatic repulsion might be responsible for the enzyme flow-through. Nevertheless, the lack of enzyme adsorption when the enzyme is negatively charged and the material is positively charged, further supports hydrophobic interactions between the SSILLP materials and ASNase purification as the most relevant type of interactions, and as previously reported by us when addressing the opposite behavior, i.e., the physical adsorption of commercial ASNase from *E. coli* onto SSILLP materials [26].

### 3.4. Semi-continuous purification of ASNase under optimized purification conditions

To assess the potential of SSILLP materials in a semi-continuous purification of ASNase, assays were performed using disposable polypropylene columns (Bio-Rad, California, USA) packed with 225 mg of [Si][$N_{3114}$]Cl under previously optimized conditions (pH 3 and S/L ratio of 15), whose results are given in Fig. 7. SILs, such as a macroporous resin functionalized with the IL 1-methyl-3-propylimidazolium chloride

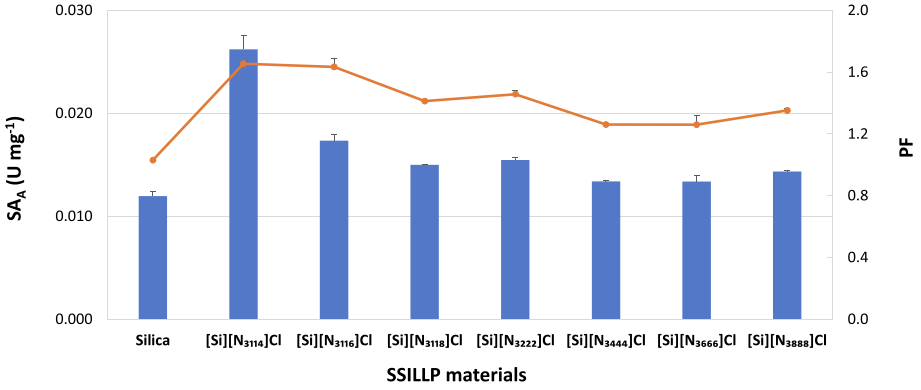


**Fig. 4.** Purification factor (PF, orange line) and specific activity of ASNase ($SA_A$, blue bars) from the supernatants after contact with activated silica and SSILLP materials with different alkyl chain lengths ([Si][$N_{3114}$]Cl, [Si][$N_{3116}$]Cl, [Si][$N_{3118}$]Cl, [Si][$N_{3222}$]Cl, [Si][$N_{3444}$]Cl, [Si][$N_{3666}$]Cl and [Si][$N_{3888}$]Cl).

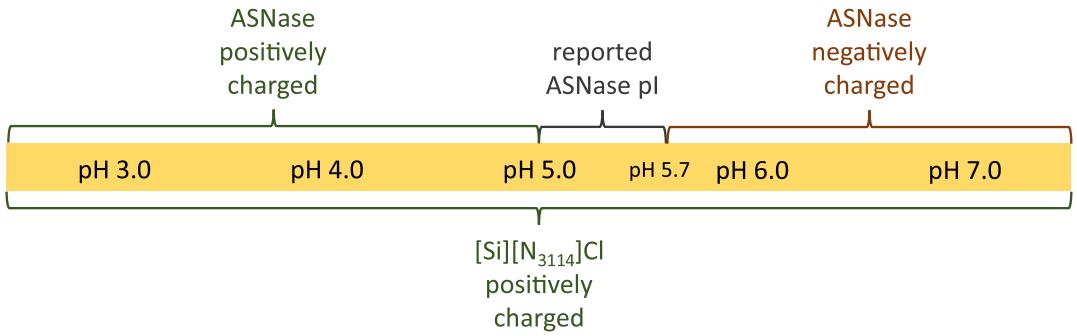


**Fig. 5.** Schematic representation of the surface charge of ASNase and [Si][$N_{3114}$]Cl between pH 3.0 and pH 7.0.

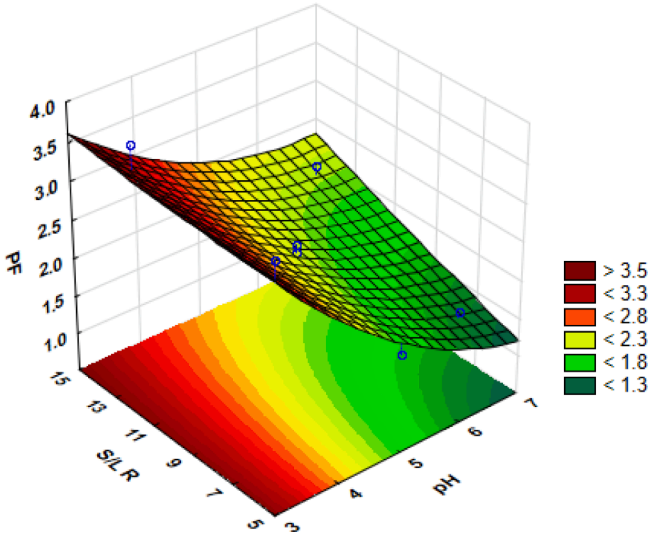


**Fig. 6.** Response surface with combined effects of pH and solid–liquid ratio (S/L R) on the ASNase purification factor (PF) using [Si][$N_{3114}$]Cl.

([$C_3C_1$im]Cl), were previously successfully applied in nucleic acids purification through a semi-continuous method [29]. However, this is the first time that SSILLP materials were applied in enzyme purification using a semi-continuous process. The purification factor and specific ASNase activity of the purified cell extract fractions ranged from 4.61 to 5.15 and from 0.042 to 0.047 U $mg^{-1}$, respectively, throughout 15 mL of enzymatic extract (Fig. 7). From the initial screening and from the batch assay under optimized purification conditions to semi-continuous assays, there were a 3.12- and a 1.53-fold increase, respectively, in the purification factor obtained. Compared to the literature, the results of this work were higher than those obtained by El-Naggar et al. [17], Hassan et al. [20] and Moharib [21], and similar to the ones attained by Abd El Baky and El Baroty [19] with non-chromatographic processes, i.e., ammonium sulfate precipitation – cf. results in Table 1. Moreover, our results are higher than those attained by El-Naggar et al. [17] and similar to the ones obtained by Hassan et al. [20] using ammonium sulfate precipitation, followed by chromatographic processes, i.e., DEAE Sepharose CL-6B ion exchange chromatography [17] and Sephadex G-100 gel filtration [20] - Table 1. Thus, our strategy to improve the purification of ASNase proved to be simple since no previous precipitation steps with salts are applied, and efficient since a purification factor of 5.15 with a specific ASNase activity of 0.047 U $mg^{-1}$ (from an enzymatic extract with a specific ASNase activity of 0.009 U $mg^{-1}$) was achieved in one step with a SSILLP operating in the flow-through like mode.

SDS-PAGE profiles of the enzymatic extract and purified cell extract fractions obtained through semi-continuous purification are given in Fig. 8. Under optimized purification conditions, the purified cell extract fractions present a clear band of the ASNase subunit at 34 kDa, which is in agreement with the profiles of commercial ASNase and the initial enzymatic extract. Moreover, most protein impurities were removed from the purified cell extract fractions, in contrast with the initial enzymatic extract. The optimized purification conditions seem to favor protein impurities aggregation as observed in the profiles of purified cell extract fractions at molecular weights superior to 245 kDa. These results suggest the combined effect of aggregation of protein impurities with

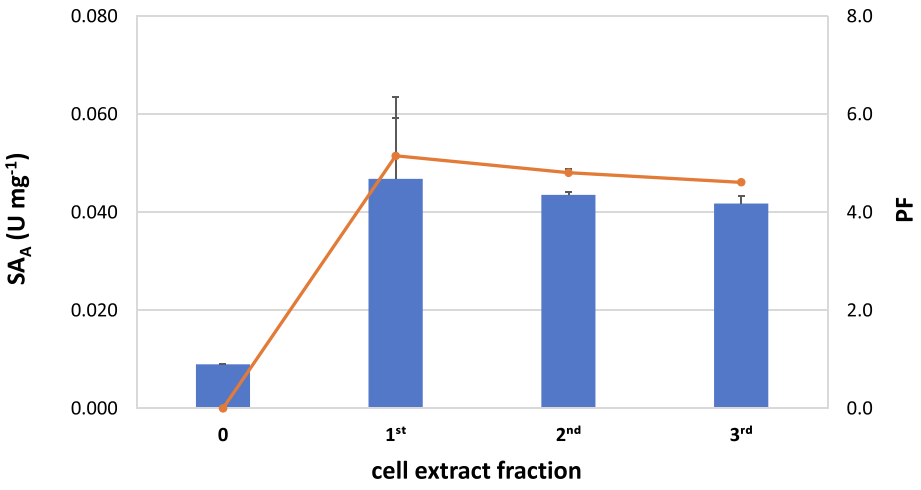


**Fig. 7.** Purification factor (PF, orange line) and specific activity of ASNase ($SA_A$, blue bars) of the separate 1st, 2nd and 3rd (5 mL) cell extract fractions recovered following semi-continuous purification of ASNase with [Si][$N_{3114}$]Cl. The first bar identified as "0" corresponds to the specific ASNase activity of the initial enzymatic extract.

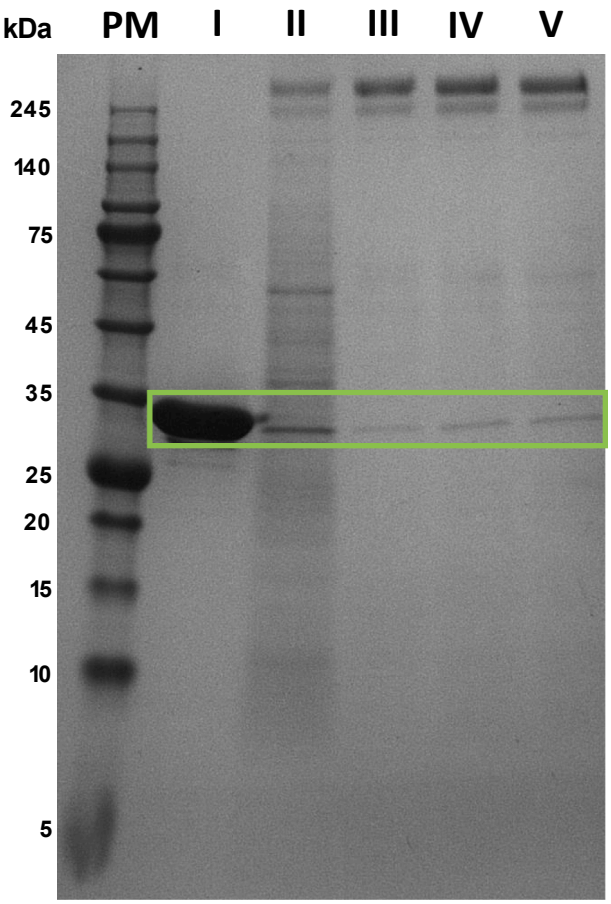


**Fig. 8.** SDS-PAGE of NZYColour Protein Marker I (PM), commercial ASNase from *E. coli* (I), enzymatic extract at pH 3 (II), 1st cell extract fraction (III), 2nd cell extract fraction (IV) and 3rd cell extract fraction (V). Cell extract fractions correspond to the separate 1st, 2nd, and 3rd 5 mL of cell extract recovered following semi-continuous purification of ASNase with [Si][$N_{3114}$]Cl. The green box highlights the band of the ASNase subunit (34 kDa). Protein concentration of 2.2 mg $mL^{-1}$ was used for the enzymatic extract to match the protein concentration of recovered cell extract fractions.

protein adsorption onto the SSILLP material.

[Si][$N_{3114}$]Cl enabled a 5.15-fold purification of ASNase, which is a promising result compared to the complex, multi-step, and expensive conventional ASNase downstream processing previously detailed. The regeneration and reusability of [Si][$N_{3114}$]Cl was assessed, but was not achieved due to the high compaction of the SSILLP material, in contrast to what was previously described for imidazolium-based materials [29,35]. However, taking into account the high cost of the pure enzyme and the low cost of SSILLP materials [25], [Si][$N_{3114}$]Cl could be applied as a single-use and disposable material for the semi-continuous purification of ASNase. Although not determined in this work, the absence of IL leaching from SSILLP materials was previously confirmed and reported by our research group [34,35], reinforcing the stability of these materials. Overall, SSILLP materials display high potential as simple and semi-continuous purification supports in enzyme flow-through downstream processing.

## 4. Conclusions

Aiming to design an alternative semi-continuous process to purify ASNase from complex enzymatic extracts, the potential of SSILLP materials composed of quaternary ammoniums and chloride as counterion was assessed. Seven SSILLP materials ([Si][$N_{3114}$]Cl, [Si][$N_{3116}$]Cl, [Si][$N_{3118}$]Cl, [Si][$N_{3222}$]Cl, [Si][$N_{3444}$]Cl, [Si][$N_{3666}$]Cl, and [Si][$N_{3888}$]Cl) were synthesized, characterized, and investigated for the first time towards ASNase purification from an enzymatic extract. An initial screening was performed and [Si][$N_{3114}$]Cl was selected as the most promising material for ASNase purification since it enabled the highest purification factor (1.65), achievable by the preferential adsorption of extract impurities. The ASNase purification conditions, namely pH (range in which enzyme is active) and S/L ratio, were optimized through Response Surface Methodology, attaining a maximum purification factor of 3.36. Semi-continuous purification of ASNase was assessed using the optimized purification conditions (pH 3 and S/L ratio of 15) enabling a purification factor of 5.15, which was achieved through the flow-through elution mode. The purification performance and low cost of SSILLP materials support their potential as alternative and simple ASNase purification materials in semi-continuous flow-through downstream processing.

Funding

This work was developed within the scope of the project CICECO-Aveiro Institute of Materials, UIDB/50011/2020, UIDP/50011/2020 & LA/P/0006/2020, financed by national funds through the FCT/MCTES (PIDDAC). This work was supported by the project POCI-01–0145-FEDER-031268-funded by FEDER through COMPETE2020, and by national funds (OE) through FCT/MCTES, and by FAPESP (2018/06908–8). Valéria C. Santos-Ebinuma acknowledges FAPESP for financial support through the project 2019/15493–9.

*CRediT authorship contribution statement*

**João C.F. Nunes:** Methodology, Validation, Investigation, Data curation, Writing – original draft, Writing – review & editing, Visualization. **Mafalda R. Almeida:** Writing – original draft, Writing – review & editing. **Gabriela B. de Paiva:** Methodology, Validation, Investigation. **Danielle B. Pedrolli:** Methodology, Validation, Investigation, Writing – review & editing. **Valéria C. Santos-Ebinuma:** Conceptualization, Methodology, Validation, Writing – review & editing. **Márcia C. Neves:** Conceptualization, Methodology, Validation, Resources, Writing – review & editing, Supervision, Funding acquisition. **Mara G. Freire:** Conceptualization, Methodology, Resources, Writing – review & editing, Supervision, Project administration, Funding acquisition. **Ana P.M. Tavares:** Conceptualization, Methodology, Validation, Resources, Writing – review & editing, Supervision, Project administration, Funding acquisition.

## Declaration of Competing Interest

The authors declare that they have no known competing financial interests or personal relationships that could have appeared to influence the work reported in this paper.

## Data availability

Data will be made available on request.

## Acknowledgments

Ana P. M. Tavares and Márcia C. Neves acknowledge FCT for the research contract CEECIND/2020/01867 and CEECIND/00383/2017, respectively. Gabriela B. de Paiva acknowledges the São Paulo Research Foundation (FAPESP) for the PhD fellowship (grant 2021/01284-9). Valéria C. Santos-Ebinuma and Danielle B. Pedrolli thank the National Council of Scientific and Technology Development (CNPq) for the fellowship grant n°312463/2021-9 and 310023/2020-3, respectively. João C. F. Nunes acknowledges SPQ and FCT for the PhD fellowship (SFRH/BD/150671/2020).

## Appendix A. Supplementary material

Supplementary data to this article can be found online at https://doi.org/10.1016/j.seppur.2023.123718.

## References


[1] A.M. Lopes, L. de Oliveira-Nascimento, A. Ribeiro, C.A. Tairum Jr, C.A. Breyer, M. A. de Oliveira, G. Monteiro, C.M. de Souza-Motta, P. de O. Magalhães, J.G. F. Avendaño, A.M. Cavaco-Paulo, P.G. Mazzola, C. de O. Rangel-Yagui, L.D. Sette, A. Converti, A. Pessoa, Therapeutic l-asparaginase: upstream, downstream and beyond, Crit. Rev. Biotechnol. 37 (2017) 82–99, https://doi.org/10.3109/07388551.2015.1120705.

[2] T. Batool, E.A. Makky, M. Jalal, M.M. Yusoff, A comprehensive review on l-asparaginase and its applications, Appl. Biochem. Biotechnol. 178 (2016) 900–923, https://doi.org/10.1007/s12010-015-1917-3.

[3] N. Verma, K. Kumar, G. Kaur, S. Anand, L-asparaginase: a promising chemotherapeutic agent, Crit. Rev. Biotechnol. 27 (2007) 45–62, https://doi.org/10.1080/07388550601173926.

[4] S. Chand, R.V. Mahajan, J.P. Prasad, D.K. Sahoo, K.N. Mihooliya, M.S. Dhar, G. Sharma, A comprehensive review on microbial l-asparaginase: bioprocessing, characterization, and industrial applications, Biotechnol. Appl. Biochem. 67 (2020) 619–647, https://doi.org/10.1002/bab.1888.

[5] J.C.F. Nunes, R.O. Cristóvão, M.G. Freire, V.C. Santos-Ebinuma, J.L. Faria, C. G. Silva, A.P.M. Tavares, Recent strategies and applications for L-asparaginase confinement, Molecules. 25 (2020) 1–28, https://doi.org/10.3390/molecules25245827.

[6] E. Kelo, T. Noronkoski, I.B. Stoineva, D.D. Petkov, I. Mononen, β-Aspartylpeptides as substrates of L-asparaginases from Escherichia coli and Erwinia chrysanthemi, FEBS Lett. 528 (2002) 130–132, https://doi.org/10.1016/S0014-5793(02)03273-8.

[7] G. Shakambari, B. Ashokkumar, P. Varalakshmi, L-asparaginase - a promising biocatalyst for industrial and clinical applications, Biocatal. Agric. Biotechnol. 17 (2019) 213–224, https://doi.org/10.1016/j.bcab.2018.11.018.

[8] J.J.M. Cachumba, F.A.F. Antunes, G.F.D. Peres, L.P. Brumano, J.C. Dos Santos, S. S. Da Silva, Current applications and different approaches for microbial l-asparaginase production, Brazilian, J. Microbiol. 47 (2016) 77–85, https://doi.org/10.1016/j.bjm.2016.10.004.

[9] A. Vimal, A. Kumar, Biotechnological production and practical application of L-asparaginase enzyme, Biotechnol. Genet. Eng. Rev. 33 (2017) 40–61, https://doi.org/10.1080/02648725.2017.1357294.

[10] A. Vimal, A. Kumar, L-asparaginase: a feasible therapeutic molecule for multiple diseases, 3 Biotech. 8 (2018) 1–3, https://doi.org/10.1007/s13205-018-1282-3.

[11] A. Furusawa, M. Miyamoto, M. Takano, H. Tsuda, Y.S. Song, D. Aoki, N. Miyasaka, J. Inazawa, J. Inoue, Ovarian cancer therapeutic potential of glutamine depletion based on GS expression, Carcinogenesis. 39 (2018) 758–766, https://doi.org/10.1093/carcin/bgy033.

[12] S.R.V. Knott, E. Wagenblast, S. Khan, S.Y. Kim, M. Soto, M. Wagner, M.-O. Turgeon, L. Fish, N. Erard, A.L. Gable, A.R. Maceli, S. Dickopf, E. K. Papachristou, C.S. D'Santos, L.A. Carey, J.E. Wilkinson, J.C. Harrell, C.M. Perou, H. Goodarzi, G. Poulogiannis, G.J. Hannon, Asparagine bioavailability governs metastasis in a model of breast cancer, Nature. 554 (2018) 378–381, https://doi.org/10.1038/nature25465.

[13] G. Baskar, K. Lalitha, R. Aiswarya, R. Naveenkumar, Synthesis, characterization and synergistic activity of cerium-selenium nanobiocomposite of fungal l-asparaginase against lung cancer, Mater. Sci. Eng. C. 93 (2018) 809–815, https://doi.org/10.1016/j.msec.2018.08.051.

[14] N. Ardalan, A.A. Sepahi, R.A. Khavari-Nejad, Development of Escherichia coli asparaginase II for the treatment of acute lymphocytic leukemia: in silico reduction of asparaginase II side effects by a novel mutant (V27F), Asian Pacific J. Cancer Prev. 22 (2021) 1137–1147, https://doi.org/10.31557/apjcp.2021.22.4.1137.

[15] F. Muneer, M.H. Siddique, F. Azeem, I. Rasul, S. Muzammil, M. Zubair, M. Afzal, H. Nadeem, Microbial l-asparaginase: purification, characterization and applications, Arch. Microbiol. 202 (2020) 967–981, https://doi.org/10.1007/s00203-020-01814-1.

[16] L.N. Ramya, M. Doble, V.P.B. Rekha, K.K. Pulicherla, L-asparaginase as potent anti-leukemic agent and its significance of having reduced glutaminase side activity for better treatment of acute lymphoblastic leukaemia, Appl. Biochem. Biotechnol. 167 (2012) 2144–2159, https://doi.org/10.1007/s12010-012-9755-z.

[17] N.E.A. El-Naggar, S.F. Deraz, H.M. Soliman, N.M. El-Deeb, S.M. El-Ewasy, Purification, characterization, cytotoxicity and anticancer activities of L-asparaginase, anti-colon cancer protein, from the newly isolated alkaliphilic Streptomyces fradiae NEAE-82, Sci. Rep. 6 (2016) 32926, https://doi.org/10.1038/srep32926.

[18] L.L. Tundisi, D.F. Coêlho, B. Zanchetta, P. Moriel, A. Pessoa Jr, E.B. Tambourgi, E. Silveira, P.G. Mazzola, L-asparaginase purification, Sep. Purif. Rev. 46 (2017) 35–43, https://doi.org/10.1080/15422119.2016.1184167.

[19] H.H. Abd El Baky, G.S. El Baroty, Optimization of growth conditions for purification and production of l-asparaginase by Spirulina maxima, Evid. -Based Compl. Altern. Med. 2016 (2016) 1–7, https://doi.org/10.1155/2016/1785938.

[20] S.W.M. Hassan, A.M. Farag, E.A. Beltagy, Purification, characterization and anticancer activity of l-asparaginase produced by marine Aspergillus terreus, J. Pure Appl. Microbiol. 12 (2018) 1845–1854, https://doi.org/10.22207/jpam.12.4.19.

[21] S.A. Moharib, Anticancer activity of l-asparaginase produced from Vigna unguiculata, World Sci. Res. 5 (2018) 1–12, https://doi.org/10.20448/journal.510.2018.51.1.12.

[22] S. Yim, M. Kim, Purification and characterization of thermostable l-asparaginase from Bacillus amyloliquefaciens MKSE in Korean soybean paste, LWT - Food Sci. Technol. 109 (2019) 415–421, https://doi.org/10.1016/j.lwt.2019.04.050.

[23] J.H.P.M. Santos, J.C. Flores-Santos, G.P. Meneguetti, C.O. Rangel-Yagui, J.A. P. Coutinho, M. Vitolo, S.P.M. Ventura, A. Pessoa Jr, In situ purification of periplasmatic L-asparaginase by aqueous two phase systems with ionic liquids (ILs) as adjuvants, J. Chem. Technol. Biotechnol. 93 (2018) 1871–1880, https://doi.org/10.1002/jctb.5455.

[24] Y. Shu, X.-W. Chen, J.-H. Wang, Ionic liquid-polyvinyl chloride ionomer for highly selective isolation of basic proteins, Talanta. 81 (2010) 637–642, https://doi.org/10.1016/j.talanta.2009.12.059.

[25] E.V. Capela, J. Bairos, A.Q. Pedro, M.C. Neves, M.R. Aires-Barros, A.M. Azevedo, J. A.P. Coutinho, A.P.M. Tavares, M.G. Freire, Supported ionic liquids as customizable materials to purify immunoglobulin G, Sep. Purif. Technol. 305 (2023), 122464, https://doi.org/10.1016/j.seppur.2022.122464.

[26] J.C.F. Nunes, M.R. Almeida, R.M.F. Bento, M.M. Pereira, V.C. Santos-Ebinuma, M. C. Neves, M.G. Freire, A.P.M. Tavares, Enhanced enzyme reuse through the bioconjugation of L-asparaginase and silica-based supported ionic liquid-like phase materials, Molecules. 27 (2022) 1–21, https://doi.org/10.3390/molecules27030929.

[27] H. Song, C. Yang, A. Yohannes, S. Yao, Acidic ionic liquid modified silica gel for adsorption and separation of bovine serum albumin (BSA), RSC Adv. 6 (2016) 107452–107462, https://doi.org/10.1039/c6ra23372d.

[28] P. Pereira, A.Q. Pedro, M.C. Neves, J.C. Martins, I. Rodrigues, M.G. Freire, F. Sousa, Efficient isolation of bacterial RNAs using silica-based materials modified with ionic liquids, Life. 11 (2021) 1090, https://doi.org/10.3390/life11101090.

[29] M.C. Neves, P. Pereira, A.Q. Pedro, J.C. Martins, T. Trindade, J.A. Queiroz, M. G. Freire, F. Sousa, Improved ionic-liquid-functionalized macroporous supports able to purify nucleic acids in one step, Mater. Today Bio. 8 (2020), 100086, https://doi.org/10.1016/j.mtbio.2020.100086.

[30] H. Qiu, S. Jiang, X. Liu, N-Methylimidazolium anion-exchange stationary phase for high-performance liquid chromatography, J. Chromatogr. A. 1103 (2006) 265–270, https://doi.org/10.1016/j.chroma.2005.11.035.

[31] E.P. Barrett, L.G. Joyner, P.P. Halenda, The determination of pore volume and area distributions in porous substances. I. Computations from nitrogen isotherms, J. Am. Chem. Soc. 73 (1951) 373–380, https://doi.org/10.1021/ja01145a126.

[32] H.B.S. Bento, G.B. Paiva, M.R. Almeida, C.G. Silva, P.J. Carvalho, A.P.M. Tavares, D.B. Pedrolli, V.C. Santos-Ebinuma, Aliivibrio fischeri l-asparaginase production by engineered Bacillus subtilis: a potential new biopharmaceutical, Bioprocess Biosyst. Eng. 45 (2022) 1635–1644, https://doi.org/10.1007/s00449-022-02769-x.

[33] A. Magri, M.F. Soler, A.M. Lopes, E.M. Cilli, P.S. Barber, A. Pessoa Jr, J.F.B. Pereira, A critical analysis of l-asparaginase activity quantification methods-colorimetric methods versus high-performance liquid chromatography, Anal. Bioanal. Chem. 410 (2018) 6985–6990, https://doi.org/10.1007/s00216-018-1326-x.

[34] S.C. Bernardo, B.R. Araújo, A.C.A. Sousa, R.A. Barros, A.C. Cristovão, M.C. Neves, M.G. Freire, Supported ionic liquids for the efficient removal of acetylsalicylic acid from aqueous solutions, Eur. J. Inorg. Chem. 2020 (2020) 2380–2389, https://doi.org/10.1002/ejic.202000101.

[35] H.F.D. Almeida, M.C. Neves, T. Trindade, I.M. Marrucho, M.G. Freire, Supported ionic liquids as efficient materials to remove non-steroidal anti-inflammatory drugs from aqueous media, Chem. Eng. J. 381 (2020), 122616, https://doi.org/10.1016/j.cej.2019.122616.

[36] J.R. Vanderveen, J. Durelle, P.G. Jessop, Design and evaluation of switchable-hydrophilicity solvents, Green Chem. 16 (2014) 1187–1197, https://doi.org/10.1039/C3GC42164C.

[37] S.K. M, S. K, Isolation and purification of high efficiency l-asparaginase by quantitative preparative continuous-elution SDS PAGE electrophoresis, J. Microb. Biochem. Technol. 3 (2011) 73–83, https://doi.org/10.4172/1948-5948.1000055.